PROCEEDINGS, 46th Workshop on Geothermal Reservoir Engineering
Stanford University, Stanford, California, February 15-17, 2021
SGP-TR-218

Crustal Fault Zones (CFZ) as Geothermal Power Systems: 3D Variation of Permeability and Related Processes

Hugo Duwiquet[1,2,3*], Laurent Guillou-Frottier[1,2], Laurent Arbaret[2], Mathieu Bellanger[3], Théophile Guillon[1], Michael J. Heap[4]

[1] BRGM, av. C. Guillemin, BP 36009, F-45060 Orléans Cedex 2, France.
[2] Univ. Orléans, CNRS, BRGM, ISTO, UMR7327 F-45071 Orléans, France.
[3] TLS-Geothermics, 91 chemin de Gabardie, 31200, Toulouse, France.
[4] Université de Strasbourg, CNRS, ENGEES, Institut Terre et Environnement de Strasbourg (ITES), UMR 7063, 5 rue Descartes, Strasbourg F-67084, France.

*hugo.duwiquet@gmail.com

Keywords: 3D permeability variations, THM numerical modeling, high-temperature geothermal energy, Crustal Fault Zone (CFZ).

ABSTRACT

The Pontgibaud Crustal Fault Zone (CFZ) in the French Massif Central provides an opportunity to evaluate the high-temperature geothermal potential of these naturally permeable zones. Previous 2D modeling of heat and mass transfer in a fault zone highlighted that a subvertical CFZ concentrates the highest temperature anomalies at shallow depths. By comparing the results of these large-scale 2D numerical models with field data, the depth of the 150°C isotherm was estimated to be at a depth of 2.5 km. However, these results did not consider 3D effects and interactions between fluids, deformation and temperature. A combined multidisciplinary approach makes it possible to better constrain the variation of permeability in 3D. This variation is then integrated into 3D numerical modeling. Based on a thermo-poroelastic assumption, a preliminary 3D THM numerical model is presented. A first parametric study highlights the role of permeability, stress direction and stress intensity on fluid flow. In particular, three different convective patterns have been identified: finger-like, blob-like and double-like convective patterns. Finally, a large-scale 3D numerical model of the Pontgibaud CFZ, based on THM coupling and the comparison with field data (temperature, heat flux, electrical resistivity), allows us to observe the convective pattern at the origin of the rise of the 150°C isotherm to economically exploitable depths. This result is obtained for values of permeability, intensity and direction of stresses comparable to the parametric study. Although simplified hypotheses have been used, 3D field data have been reproduced. Finally, we tried to understand the observed effects of poroelasticity on fluid flow.

1. INTRODUCTION

As potential renewable and economical resources, Crustal Fault Zones (CFZ) remain largely unexplored and therefore unexploited. Widely present on Earth (Scibeck, 2020), these naturally permeable zones have all the characteristics of a potential reservoir for high-temperature geothermal energy and therefore offer significant energy potential over the world. Moreover, these naturally permeable and deep zones would limit the use of hydrofracturing and/or hydroshearing that could induce seismic events that have disrupted geothermal projects or suspended operations (Deichmann and Giardini 2009, Evans et al., 2005). Since 2014, TLS-Geothermics, a French company involved in geothermal exploration, has been keen to demonstrate the viability of CFZ as a geothermal exploration play for economic power generation.

This kind of reservoir is currently poorly constrained, probably due to a lack of understanding of the primary geological factors controlling the occurrence of this type of geothermal play. In order to facilitate exploration, it seems necessary to be able to dissociate the key parameters favoring the ascent of hot fluid to economically attractive depths. Previous studies have shown that vertical deep deformation zones, could concentrate the most important temperature anomalies at the lowest depths (Duwiquet et al., 2019; Guillou-Frottier et al., 2020). Our recent results suggest that vertical deformation zones oriented at 30 and 70° relative to maximum horizontal stress could correspond to potential targets for high-temperature geothermal energy (Duwiquet et al., 2021). Permeability variation in crustal domain has been widely discussed since the 1990s (Martel, 1990). Overall, the permeability variation of CFZ is primarily controlled by the coupling between Thermal (T), Hydraulic (H), Mechanical (M), and Chemical (C) processes (Horne, 1979; Parry et al., 1988; Barton et al., 1995). Permeability can be considered as a static and isotropic parameter in space. Different studies have reproduced field data by considering fixed fault permeabilities around 10^{-14} m^2 (Guillou-Frottier et al., 2013; Magri et al., 2016). For large-deformation fault zones field data from the Pontgibaud CFZ have been reproduced by considering a static but variable permeability in different space dimensions. (Duwiquet et al., 2019; 2020; 2021). However, permeability has been recognized as a dynamic parameter evolving in time and space as a result of the various geological processes (Sibson et al., 1988; Ingebritsen and Gleeson, 2015).

In this study, we first propose additional field observations to better constrain permeability variation in the three dimensions. This variation in permeability will be integrated into a 3D coupled THM numerical modeling where a thermo-poroelastic hypothesis is assumed. These results will be compared with field data. Our multidisciplinary approach will facilitate the understanding of how fluids can circulate within a naturel system. Finally, a 3D numerical study with THM coupling and dynamic permeability will attempt to approach the different processes that can control the fluids circulation within a fault.

2. GEOLOGICAL SETTING

The “La Sioule” licence area (black contour in Figure 1) is located to the West of the Limagne graben in the Massif Central (France), in a Paleozoic basement domain and is partially covered by the northern part of the Cenozoic volcanic formations (in blue in Figure 1). It is bounded to the West by the Sillon Houiller fault zone, to the South by the volcanic massif of the Monts Dore, and to the North and East by the granitic massif of Saint-Gervais and the Chaîne des Puys volcanic chain, respectively. Variscan metamorphic formations (ortho and para-migmatites, orthogneiss, paragneiss and mica schists) are mainly present in the area (in green in Figure 1). Carboniferous plutonic rocks are characterized by monzogranite and granodiorite (red in Figure 1) and Viseo-Serpukhovian volcano–sedimentary formations (brown in Figure 1). Upper Pennsylvanian and Permian detritic sedimentary formations mark the late Variscan basins emplaced on the major crustal fault zone.

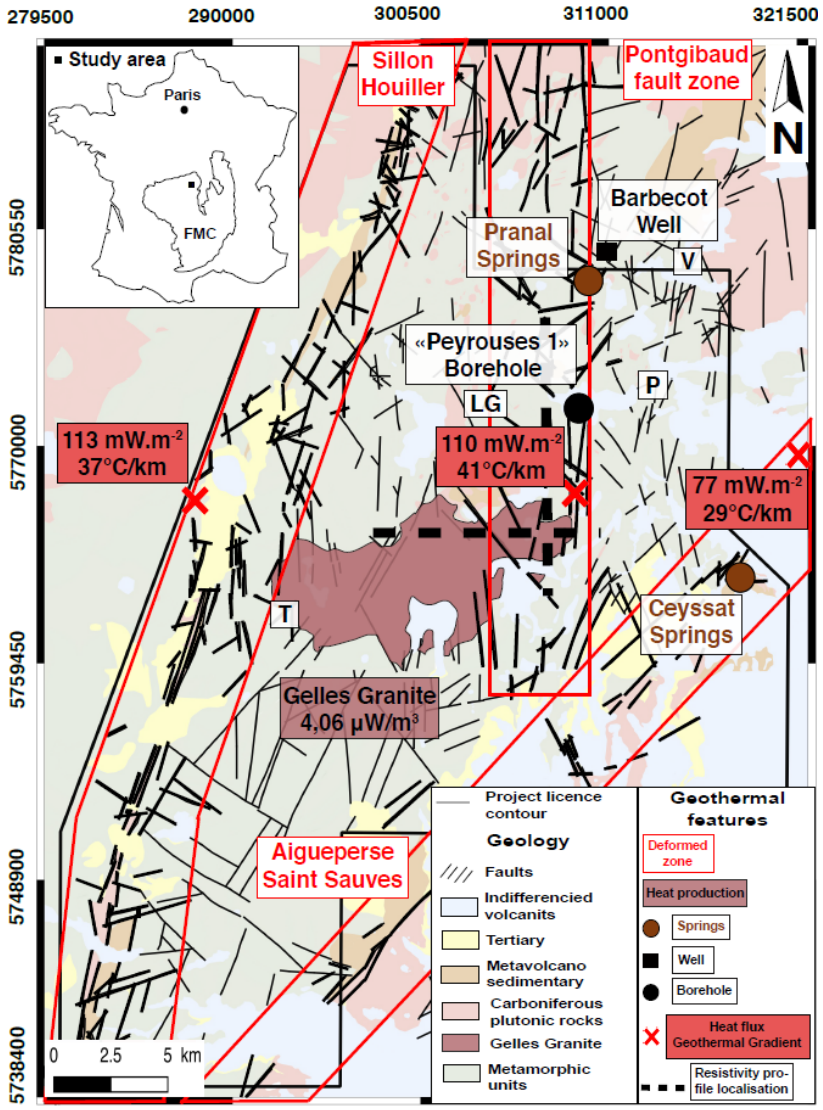

Figure 1: Geological and geothermal features in the “La Sioule” licence area (black contour), French Massif Central (FMC). Heat flow and geothermal gradient (red crosses) are from, Lucazeau and Vasseur (1989), International Heat Flow Commission. Heat production (is from Lucazeau, 1981) and resistivity profile (black dashed line) from Ars et al. (2019). P: Pontgibaud. LG: La Goutelle. V: Villelongue. T: Tortebesse. Coordinate system: WGS84 Pseudo-Mercator EPSG: 3857 (After the 1/50,000th geological map published by BRGM). Modified after Duwiquet et al. (2019, 2020).

Bounded to the East and West by the Aigueperse-Saint-Sauves fault and the Sillon Houiller fault, the “La Sioule” licence is largely affected by late Variscan tectonics. The Pontgibaud Crustal Fault Zone is a more than 40 km long system pinched between the Sillon Houiller and the Aigueperse-Saint-Sauves fault zones (Figure 1). The evidence of current fluid circulation is indicated by the presence of springs (Ceyssat and Pranal springs, Figure 1).

Several seismological stress-state evaluations were performed around the studied area. Mazabraud et al. (2005) determined that the maximum horizontal stress axis is oriented close to NW-SE. More recently local stress-states evaluated by TLS-Geothermics and

processed by MAGNITUDE (a Baker Hughes company) indicated that direction of the maximum stress axes are bracketed between N135° and N150° (for more details see Duwiquet et al., 2021).

3. OBSERVATIONS AND MEASUREMENTS OF PERMEABILITY SPATIAL VARIATION (X, Y, Z)

3.1 Field, thin-section and X-ray microtomography observations for permeability spatial variations (X, Y)

When examining different outcrops of the Pontgibaud Crustal Fault Zone, all lithologies show a large range of facies from unaltered and undeformed rocks to altered and/or fractured rocks. Breccia, fractured zones, cataclasites and mineralized veins are noteworthy (see Figure 2). These mineralizations are markers of the paleo-circulation of fluids. Samples were acquired from the "Peyrouses 1" borehole located within the Pontgibaud fault system (see Figure 1). Microstructural observations made on thin sections of these samples mainly show fractured and altered facies. Voids are located within the fracture networks (present in red, Figure 2). Some of these fractures are totally sealed, and therefore may provide barriers to fluid flow, while others show voids, thus conferring a potential permeability to the system. We therefore observed evidence for potentially high- and low-permeability zones within the fault system.

Secondary mineralization is present at the borders of voids, thus ruling out the possibility of an anthropogenic origin of these voids during the manufacturing process of the thin sections. At this scale of observation, all the fractures seem to form a dendritic network. This type

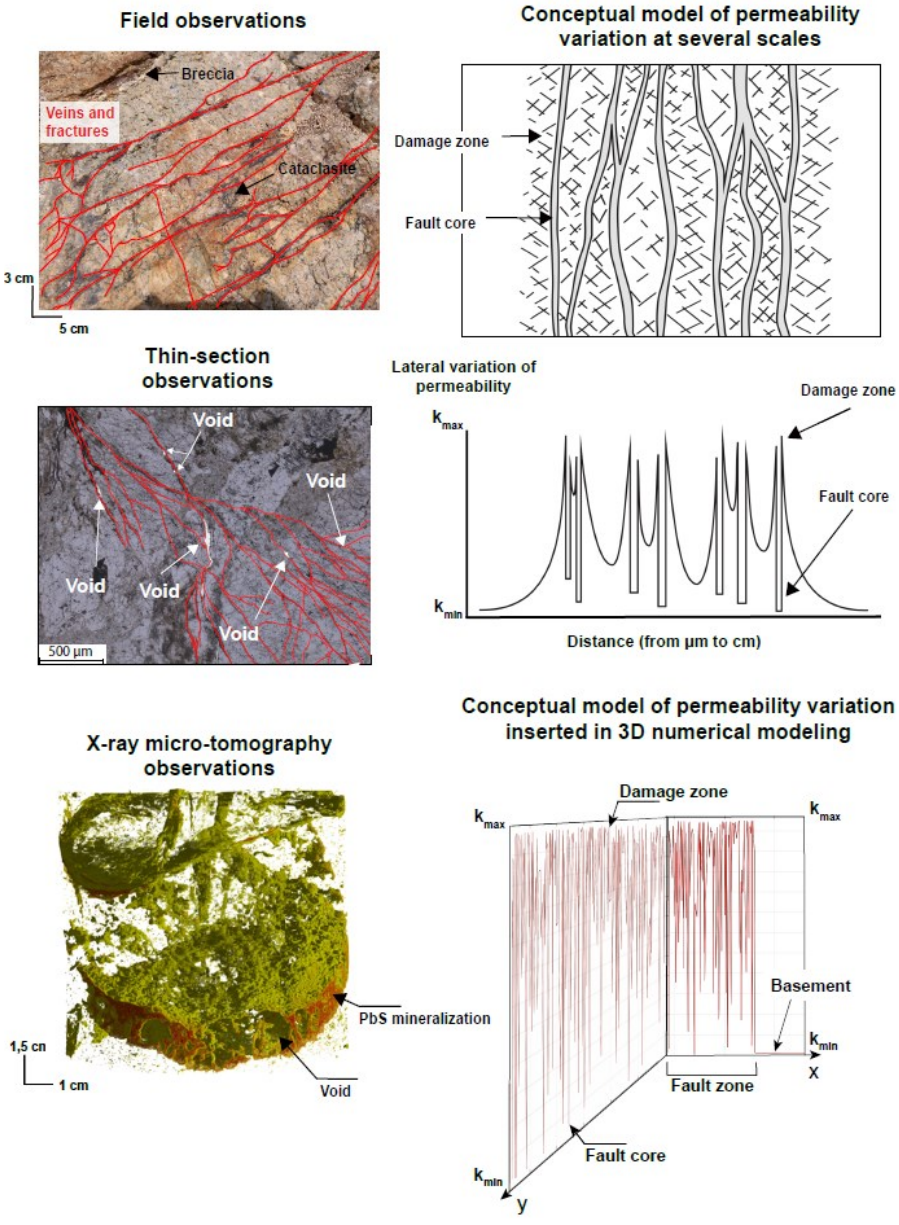

Figure 2: Field and laboratory observations (left). Incorporation of the multiple fault core conceptual model (Faulkner et al., 2010) within numerical modelling done with Comsol Multiphysics™ (right). The resolution of the microtomographic image is 10 μm.

of network is largely detailed in the literature (Reis, 2006; Lorenzini et al., 2011) and would be present in systems with intense fluid circulation (Bejan and Lorente, 2006).

In order for fluids to circulate, it is necessary that these voids are connected in the three dimensions of space. In order to verify this, the same samples were scanned and analyzed by X-Ray computed tomography at the Institute of Earth Sciences in Orleans (ISTO). The 3D observations (see bottom left in Figure 2) show, in yellow, the walls of mineralizations in which some voids are taken into account and in red the mineralization (here galena (PbS)). The presence of voids is marked at the heart of some mineralizations and at the levels of the mineralization walls. Moreover, these planes seem to be connected in the three dimensions, thus potentially facilitating the fluids circulation.

The conceptual model of Faulkner et al. (2010) describes damage zones (high permeability zone) and fault cores (low permeability zone). Considering the close correspondence between the variations in potential permeability of the different observations made with the conceptual model of Faulkner et al. (2010), we propose to integrate this permeability variation into our numerical models along the two axes, x and y (see Figure 2). Equations 1 and 2 include a lateral variation of permeability within the fault zone in order to virtually reproduce the high permeability zones (damage zones) and low permeability zones (fault cores). While this model appears consistent with the model of Faulkner et al. (2010), other conceptual models of permeability variations in a fault zone may exist (Mitchell and Faulkner, 2012). The latter seems to be better suited to our field data. If the variations along the x and y axes could be constrained, variation along the z-axis and quantification of this range of permeability variation would provide additional qualitative and quantitative information.

3.2 Borehole observations and permeability measurements for permeability spatial variations (X, Z)

Sampling was made on different lithological facies present in the "Peyrouses 1" borehole. Permeability measurements have been performed at the Strasbourg Institute of Earth and Environment (SITES), in Strasbourg (France). For more details on the protocol used, see Heap and Kennedy 2016. The averages values of the permeability on intact, fractured, altered, fractured and altered facies are of 2.8×10^{-16}, 3.9×10^{-15}, 1.5×10^{-15}, 3.1×10^{-13} m^2, respectively. In order to observe these permeability variations according to the different facies and depth, we have transcribed these average values into a permeability/depth profile (Figure 3). This profile provides additional constraints on the variation of permeability from 0 to 250 m. We can then try to incorporate these permeability variations into our numerical model.

Depth-dependence of permeability follows the equation of Garibaldi et al. (2010). This equation makes it possible to consider the effect of compaction on permeability. Local variations in permeability are additionally given by equation 2. By zooming in on the first 250 meters, permeability variations in the order of 10^{-16} to 10^{-13} m^2 can be observed (Figure 3). This variation is of the same order of magnitude

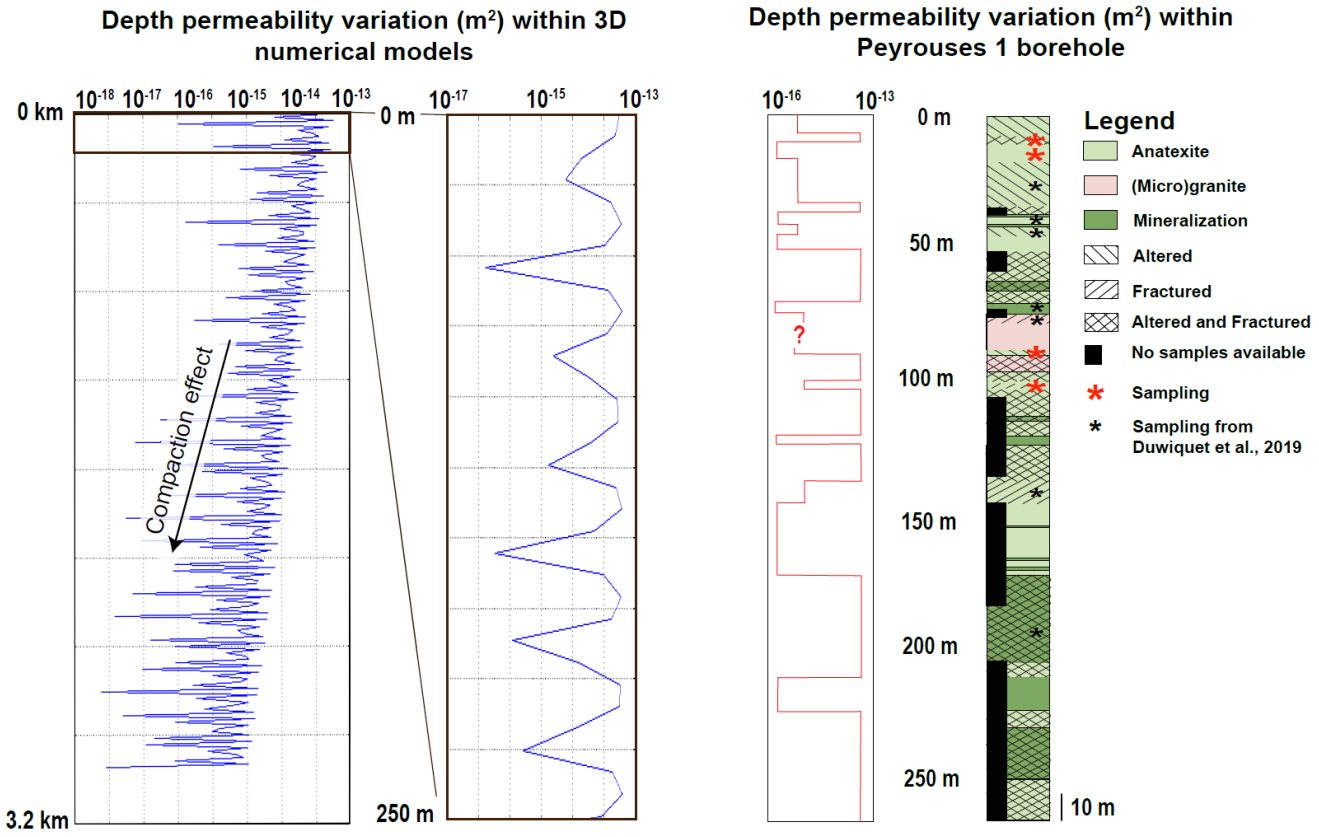

Figure 3: Variation in permeability along the x and z axes and comparisons with the average permeability value of samples representing different facies taken from the Peyrouses 1 borehole (see location Figure 1).

as the one measured in the laboratory. It is not surprising that the permeability variation of the numerical models does not exactly follow the variations present in the borehole. Moreover, the figures do not exactly reflect the exact values, since we have inserted the averages of these measured values. Nevertheless, we will keep the assumption that the general trends are respected.

4. NUMERICAL MODELING

Numerical simulations were run with Comsol Multiphysics™ software. Here we couple the heat and mass transfers with the poroelastic interface. This interface combines the regular fluid flow formulation with linear elastic solid mechanics of the porous medium matrix. Poroelasticity coupling means that the pore volume fraction can be affected by external stress. Voids filled with fluids change in pressure, resulting in fluid movement. The material will deform elastically as a consequence of this stress and the change in void volume. This interface includes an expression of the stress tensor as a function of the strain tensor and the Biot-Willis coefficient. Details on the used equations used can be found in Duwiquet et al. (2021).

These numerical models will consist of integrating the observations previously made. First, an idealized and simplified case including different parameters such as the intensity and direction of the stress, or the permeability, will be tested. Particular attention will be paid to the convective pattern. Second, a more realistic model including field data issued from the natural Pontgibaud system will be performed. The results of the numerical modeling will be compared with other field data, and this comparison will allow to identify of convective pattern and its comparison with the parametric study. Stress effects will be observed on the fluid flow. A calibration step will be carried out in order to verify the use of version 5.5 of the Comsol Multiphysics™ code with other numerical codes. Finally, in order to approach the processes at the origin of the modifications in the circulation of fluids, a dynamic function of permeability adapted to fractured media will be integrated.

4.1 3D permeability variation

Field and laboratory analyses indicate that the Pontgibaud area has a very high fracture density. By keeping the usual depth-decrease of permeability, a lateral variation can be included, by using the following spatial variation:

$$K_F(x,y,z) = K_{F0} \times f(z) \times f(x,y,z) \quad (1)$$

Here $K_F(x,y,z)$ is the fault permeability (in m^2) dependent on the three space directions. K_{F0} is the permeability at the surface, $f(z)$ is the depth-dependent function and $f(x,y,z)$ makes the permeability alternate along a sinusoid applied to the three axes of the numerical model, such as:

$$K_F(x,y,z) = K_{F0} \times \left[exp\frac{z-800}{\delta}\right] \times \left[101 + 100 \times \sin\left(2 \times \pi \times \frac{(x+y+z)}{\lambda}\right)\right] \quad (2)$$

The term λ corresponds to the wavelength of the sinusoid. To reproduce rather fine alternations of high and low permeability, as suggested by field and laboratory observations (see Figure 2), a low value (10^{-5}) for the term λ was chosen (Duwiquet et al., 2019; 2020; 2021). The length δ (m) characterizes the intensity of the decrease in permeability with depth, taken here at 2500 m.

4.2 Parametric study: effect of stress intensity, stress direction and permeability on fluid flow

We will consider two different numerical experiments. The first considered a very simplified and idealized geometry, where a vertical deformation zone is located in the middle of a basement. We will look at the role of stress intensity and direction as well as permeability on fluid flow and their effects on the intensity and depth of temperature anomalies. To do this, the direction of the deformation zone varies from 0 to 90° (with a 10° step), and the intensity of the main stress varies from 0 to 100 MPa (with a 10 MPa step). The permeability K_{F0} of the fault varies from 1×10^{-16} to 4×10^{-14} m^2 (with a 10^{-16} m^2 step). The permeability of the basement will be fixed in all our models at $K_{b0} = 10^{-16}$ m^2. (for more details on boundary conditions, see Duwiquet et al., 2021). In order to account for both permeability of the fault and of the basement, the R ratio is defined by:

$$R = \frac{K_{fmax}}{K_{bo}} \quad (3)$$

This ratio compares the maximum permeability of the fault and of the basement. Other K_{b0} values have been tested but higher values are not realistic and lower values do not change the results detailed below. The purpose of this first step is to unbundle different parameters that may influence the fluid flow.

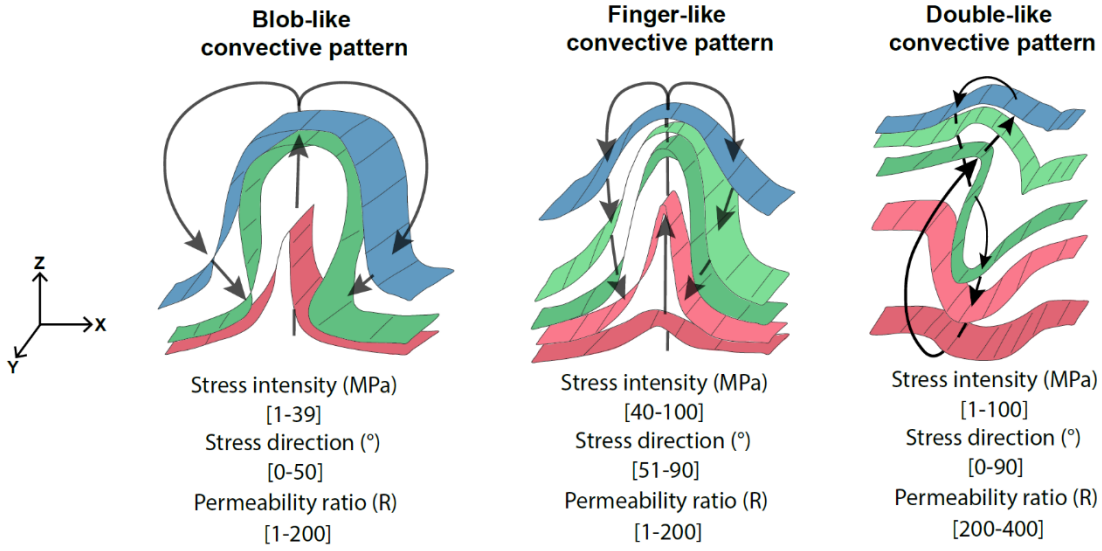

Figure 4: Results of the parametric study. On the whole of the calculations made (n > 2,500) three convective patterns are observable: the blob-like, the finger-like and the double-like patterns. These three patterns depend on parameters such as permeability ratio, direction and intensity of the stress.

Three convective patterns are observed: blob-like, finger-like and double-like convective pattern (Figure 4). Each of these patterns can be found for ranges of the tested parameters. Looking at the permeability ratio we find two different convective patterns for the lowest ratios tested R [1-200]. It would seem that for low permeability ratios, the evolution from a blob-like pattern to a finger-like pattern is controlled by the other parameters, such as the intensity and direction of the stress. With higher permeability ratios R [200-400] we observed only one convective double-like pattern. Thus, it would seem that for high permeability ratios, the intensity and direction of the stress have no effect on fluid flow. This does not seem to be the case for the other two convective patterns.The blob-like convective pattern is obtained for stress intensity values between 1 and 39 MPa and directions between 0 and 50°. We observe finger-like convective pattern for stress intensity values between 40 and 100 MPa and directions between 51 and 90°. Therefore, with a thermo-poroelastic hypothesis and for low permeability ratios, the intensity of a stress and its direction in relation to the deformation zone plays a significant role on fluid flow patterns.

4.3 Numerical modeling of a natural system: the case of the Pontgibaud CFZ

The second numerical experiments will involve 3D THM numerical modelling of the Pontgibaud crustal fault zone. Each lithology will be assigned its own physical and thermal properties. Concerning the mechanical boundary conditions, we propose to use in situ measurements from the Chassoles borehole (located 60 km South-East of Pontgibaud). The objective of this second step is to integrate the set of observations and properties specific to Pontgibaud. Whether for the first parametric study or the second study on the Pontgibaud hydrothermal system, the Young's moduli chosen for the basement and deformation zone are 60 GPa and 5 GPa, respectively (Cappa and Rutqvist, 2011). For more details on boundary conditions, geometries and physical properties, see Duwiquet et al. (2021).

The distinction between these three convective figures can be a determining factor in estimating the volume of the geothermal reservoir. For example, the volume occupied by the blob-like isotherms will be larger than the volume occupied by the finger-like convective pattern isotherms. If we were able to parametrically determine three convective patterns, it would be interesting to compare these results with models of natural systems integrating field and laboratory observations and measurements.

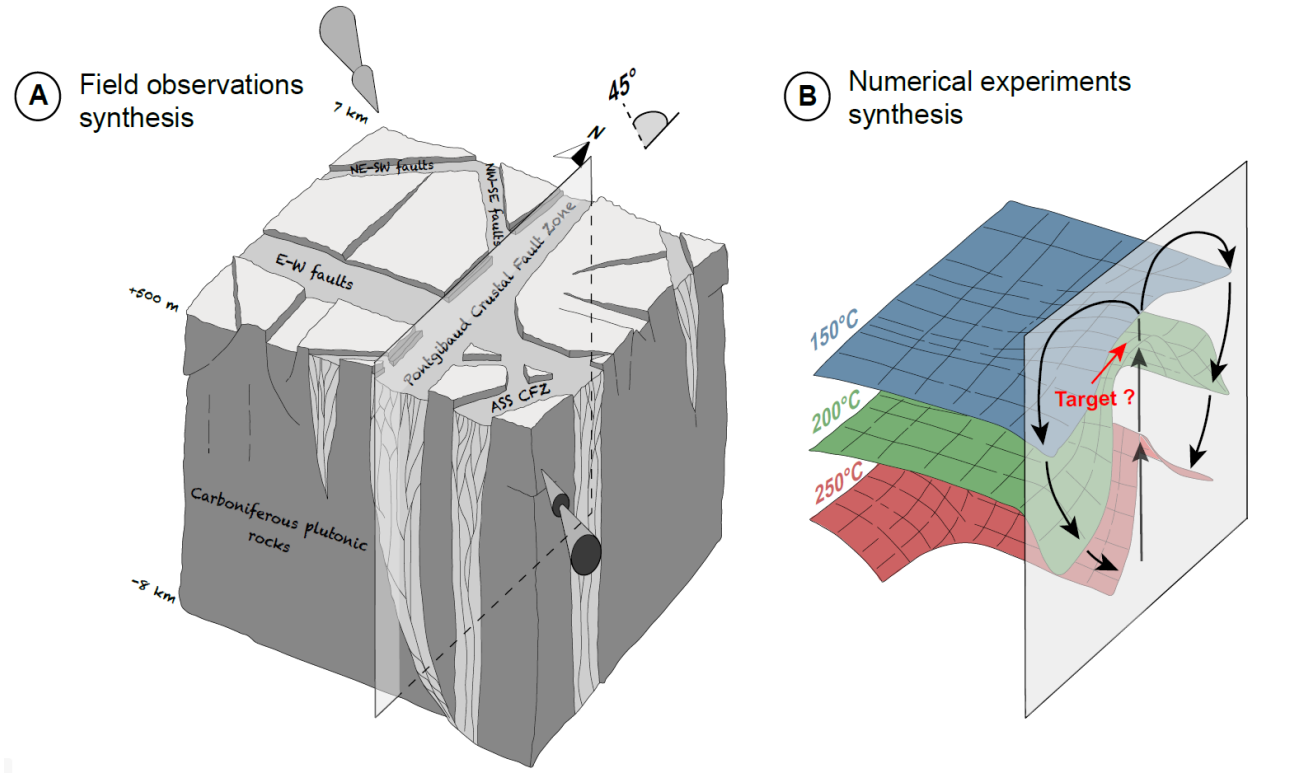

Figure 5: [A] Synthesis of field observations and numerical experiments. The Pontigbaud CFZ is a large deformation zone whose geophysical data (Ars et al., 2019) show deep rooting. [B] The results of the numerical experiments and the comparison with the geothermal gradient and heat flow show that a blob-like fluid circulation would be effective within the Pontgibaud CFZ.

The global geometry of the Pontgibaud system is synthesized in Figure 5A. It includes structural measurements made by TLS-Geothermics and discussed in Duwiquet et al. (2021). The Pontgibaud system is characterized by a large deformation zone comprising different fault families (Duwiquet et al., 2019). The observations and field measurements point to a system that allow fluids to circulate to great depths. Numerical modeling of this system shows that for a maximum permeability value imposed within the Pontgibaud fault zone of to 1×10^{-14} m^2, the 150°C isotherm would be at a depth of 2.3 km.

The resistivity profiles established by Ars et al. (2019) show a negative resistivity anomaly between 3 and 4 km in depth. This anomaly may be related to the presence of metals, clays, or the presence of hot fluid. Compared to the results obtained with numerical modeling a positive temperature anomaly is estimated at a depth between 2 and 3 km. Moreover, these results show a geothermal gradient of 41°C.km^{-1} and a heat flux of 110 mW.m^{-2}, at the location where they were measured and estimated in the field to be 41.5°C.km^{-1} and 110 mW.m^{-2}.

This 150°C rise in the isotherm (Figure 5B) is the consequence of fluid ascending to the center of the Pontgibaud CFZ and descending at its extremities. This convective pattern was defined in the study as the blob-like convective pattern (see Figure 4). This convective pattern was, in the parametric study, obtained for permeability ratios R[1-200], stress intensities below 39 MPa, and an orientation with respect to the main stress between 0 and 50°. When comparing these three parameters, the convective pattern observed in the numerical model of the Pontgibaud area is comparable with the result from the parametric study.

Hence, in these two first approaches, we distinguished three different convective pattern, which we were able to compare to a natural system constrained by field data. However, no process was demonstrated that could explain for example the origin of the difference between the blob-like and finger-like convective pattern. We will start by checking the code of Comsol Mulitphysics™ version 5.5 with the OpenGeoSys codes (Magri et al., 2017) as well as version 3.5a of Comsol Multiphysics™ (Guillou-Frottier et al., 2020).

4.4 Benchmark experiment

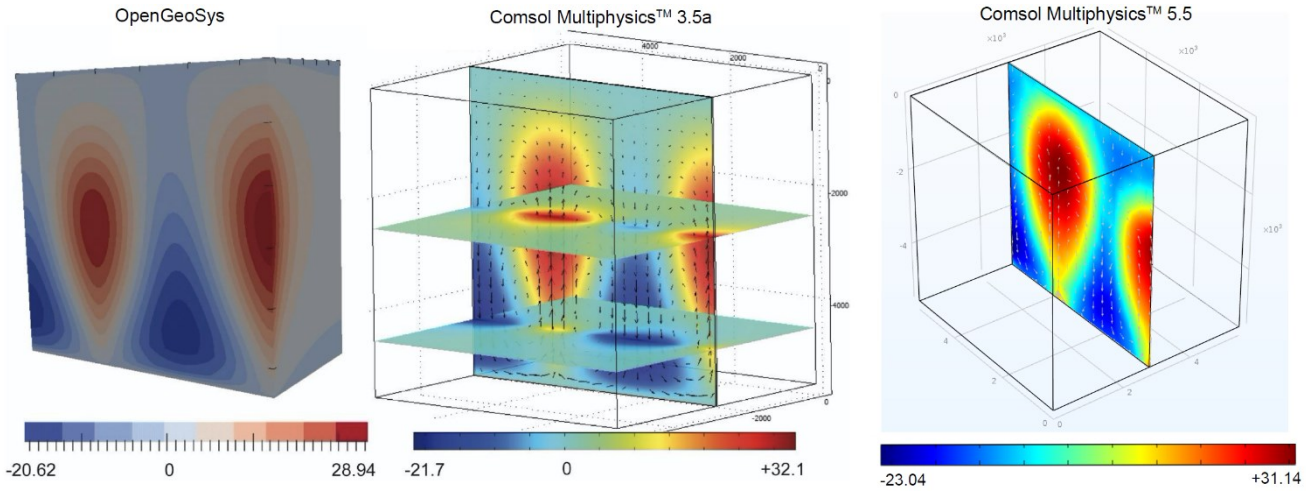

Figure 6 : Benchmarking of our numerical experiments with the OpenGeoSys code (Magri et al., 2017) and Comsol Mulitphysics™ V3.5a (Guillou-Frottier et al., 2020).

The calibration of our numerical experiments has been realized on the basis of results from version 3.5a of Comsol Multiphysics™ (Guillou-Frottier et al., 2020) as well as from the OpenGeoSys numerical code (Magri et al., 2017). These models consider a 40 m wide vertical fault in an impermeable box (a cube of 5.5 km on each side). The fluid properties are identical for all three results. A linear dependence of temperature on water density, and an exponential decrease in viscosity with temperature. This result is shown for a time $t_0 + 10^{13}$ s. The permeability value is fixed and imposed at 5×10^{-15} m^2. The maximum flow velocity of the fluids is 2.03×10^{-9} m.s^{-1}. The flow velocity of the fluids is higher than that described by Guillou-Frottier et al. (2020) who record a velocity of 1.4×10^{-9} m.s^{-1}. The convective patterns are similar. The fluid velocity accelerates along the permeable fault and exhibits upward movements due to the temperature gradient and buoyancy forces associated with lower water density at depth. The thermal disturbances are also in the orders of magnitude of the previous studies -23.04 and +31.14 °C.

The numerical experiments of Magri et al. (2017) and Guillou-Frottier et al. (2020) use Darcy's law in conjunction with the equations of heat. The following numerical experiments couple the equations of heat and mass transfer with the modulus of poroelasticity. The poroelasticity interface of Comsol Multiphysics™ combines Darcy's law with the linear elastic behavior of porous media. Poroelastic coupling allows boundary stresses to be imposed, which can be recorded as fluid pressure. In Figure 6 (right), no stress or other mechanical conditions are applied. Consequently, this experiment correspond to an identical coupling as in the previous studies (figure 6, left and middle cases).

4.4 Variation of fault permeability with a thermo-poroelastic assumption

In order to try to understand the processes that can act on the fluids flow (see Figure 4), we will integrate a relationship between porosity and permeability. For this, the Kozeny-Carman relationship in which permeability is proportional to the cube of porosity does not seem appropriate for fractured systems. Based on empirical work, Parisio et al. (2019) make a link between a permeability of a fully fractured system k_f with a permeability of an intact system k_i and the porosity n. This relationship is written in the form:

$$\log k = (1 - \omega) log k_i + \omega log k_f \quad (4)$$

With

$$k_i = 4.979 \times 10^{-11} n^{3.11} \quad (5)$$

and

$$k_f = 1.143 \times 10^{-11} n^{0.64} \quad (6)$$

In this relation n is the porosity ($n = 0.1$) and ω is a parameter representing a fully fractured system ($\omega = 1$), or an intact system ($\omega = 0$). Here $\omega = 0.8$ (for more details see Parisio et al., 2019).

We will impose an arbitrarily chosen stress of 15 MPa, on the side of the cube. By its application and its intensity, this boundary condition does not transcribe the natural evolution of the constraint with depth. It could nevertheless allow us to consider the first order effects of this stress on permeability.

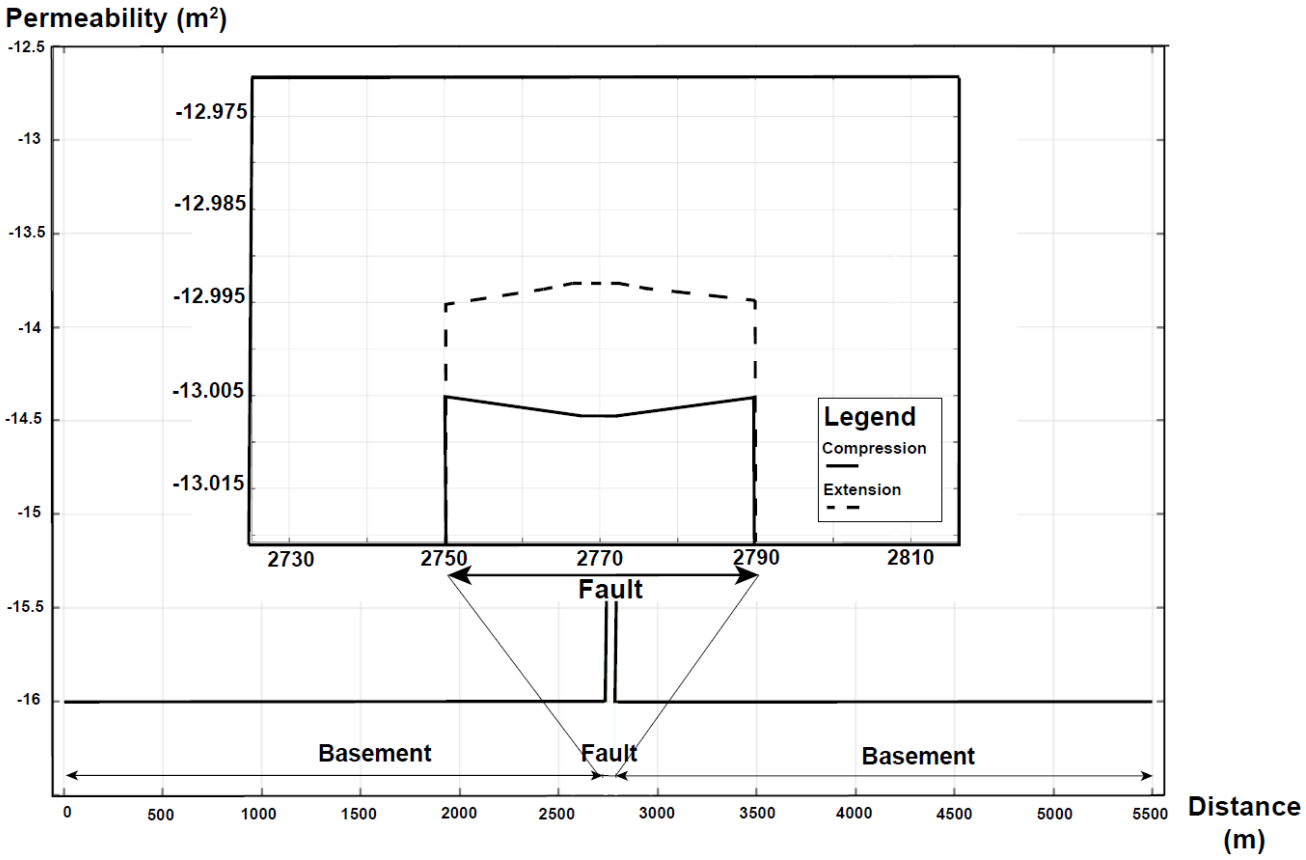

Figure 7 : Permeability variation within the basement and fault for compressive and extensive boundary conditions (+/-15 MPa).

The results of the numerical experiments show no permeability variation within the basement, which remains fixed at 10^{-16} m^2. Within the fault, for a compressive boundary condition, the permeability is $10^{-13,005}$ m^2 at the extremities of the fault and $10^{-13,008}$ m^2 at the center of the fault. For an extensive boundary condition, the permeability at the extremities of the fault is $10^{-12,995}$ m^2 and the permeability at the center of the fault is $10^{-12,997}$ m^2. The consequence of applying a 15 MPa compressive stress will slightly decrease the permeability. Conversely, the application of a 15 MPa stress in extension will slightly increase the permeability.

This different response of permeability to the stress application can be explained by the difference in Young's modulus. As in other numerical models, the value of 60 GPa is imposed to the basement and 5 GPa to the fault (Cappa and Rutqvist 2011). The response to the mechanical effects of permeability may then be greater in the fault than in the basement. In the fault, the results of this variation in permeability may be the consequence of compression or stretching of the porosity.

In a natural case, the variation in permeability in the interseismic phase varies by 25% around 4×10^{-14} m^2 (Ma et al., 2019). Here we can see with a thermo-poroelastic hypothesis a variation in permeability of less than 1%. At this stage, the question that can be asked is whether this tiny variation can have a role on fluid circulation. Even if these mechanical boundary conditions are not legitimate in a natural system, where the stress decreases with depth, it does allow a small variation in permeability to be highlighted when a stress is applied.

5. CONCLUSIONS AND PERSPECTIVES

Observations and measurements, both from the field and the laboratory constrained the permeability variations imposed in the numerical models. These observations highlight succession of high permeability and of low permeability zones. This variation in permeability within CFZ corresponds to the conceptual model of Faulkner et al. (2010), in which they present a variation in the space of the damage zone (high-permeability) and fault core (low-permeability). These observations, related to a conceptual model, allow us to constrain the lateral variations in permeability. The average values of laboratory permeability measurements made on the different lithologies present in the Peyrouses 1 borehole vary from 2.8×10^{-16} to 3.1×10^{-13} m^2. The transcription of these values within the borehole allowed us to constrain the permeability variation with depth. Finally, through observations and measurements, we were able to constrain the permeability variations of a CFZ modelled with Comsol Multiphysics^{TM} in all three spatial dimensions. On the basis of a thermo-poroelastic hypothesis, the first step of the numerical modeling consisted of dissociating the role of permeability, intensity and direction of a stress on fluid flow. After more than 2,500 runs, three convective forms were observed: the blob-like convective pattern, the finger like and the double like convective pattern. The shape of these convective patterns can have an significant impact on the volume of the geothermal reservoir. At this stage, the second step was to model a natural system in order to see if, by integrating values of permeability, intensity and direction of stress, the convective patterns observed by the parametric study could be found. The blob like convective pattern is found on the result of the large-scale numerical modeling, for values of permeability, intensity and direction of stress consistent with the ranges obtained during the parametric study. By an upward movement of the fluids at the center of the system, this convective pattern moves up the 150°C isotherm to a depth of 2.3 km. Although it was possible to reproduce field data from this numerical modeling, it did not allow us to understand the observed effect of the application of a stress on the circulation of fluids.

In order to understand possible processes at work we calibrated our numerical models and then considered that they no longer have a static (even if variable in the three dimensions of space) but dynamic permeability adapted to fractured mediums. When a simplified horizontal stress is applied, we observe a permeability variation of less than 1%. Futher studies will decipher whether this small variation could cause changes in convective patterns.

REFERENCES

Ars, J. M., Tarits, P., Hautot, S., Bellanger, M., Coutant, O., Maia, M.: Joint inversion of gravity and surface wave data constrained by magnetotelluric: application to deep geothermal exploration of crustal fault zone in felsic basement, *Geothermics*, 80, (2019), 56-68.

Barton, C. A., Zoback, M. D., Moos, D.: Fluid flow along potentially active faults in crystalline rock, *Geology*, 23(8), (1995), 683-686.

Bejan, A., and Lorente, S.: Constructal theory of generation of configuration in nature and engineering, *Journal of applied physics*, 100(4), (2006), 5.

Cappa, F., and Rutqvist, J.: Modeling of coupled deformation and permeability evolution during fault reactivation induced by deep underground injection of CO2, *International Journal of Greenhouse Gas Control*, 5(2), (2011), 336-346.

Deichmann, N., and Giardini, D.: Earthquakes induced by the stimulation of an enhanced geothermal system below Basel (Switzerland), *Seismological Research Letters*, 80(5), (2009), 784-798.

Duwiquet, H., Arbaret, L., Guillou-Frottier, L., Heap, M. J., Bellanger, M.: On the geothermal potential of crustal fault zones: a case study from the Pontgibaud area (French Massif Central, France), *Geothermal Energy*, 7(1), (2019), 33.

Duwiquet, H., Guillou-Frottier, L., Arbaret, L., Bellanger, M., Guillon, T., Heap, M,-J.: Crustal Fault Zones (CFZ) as geothermal power system: a preliminary 3D THM model constrained by a multidisciplinary approach. *Geofluids*, in press, 2021.

Duwiquet, H., Guillou-Frottier, L., Arbaret, L., Guillon, T., Bellanger, M., & Heap, M.: Crustal Fault Zone: New geothermal reservoir? Structural dataset and preliminary 3D TH (M) modelling of the Pontgibaud fault zone (French Massif Central). In 45th Workshop on Geothermal Reservoir Engineering, Stanford University, Stanford, CA (2020).

Evans, K. F., Moriya, H., Niitsuma, H., Jones, R. H., Phillips, W. S., Genter, A., ... & Baria, R.: Microseismicity and permeability enhancement of hydrogeologic structures during massive fluid injections into granite at 3 km depth at the Soultz HDR site, *Geophysical Journal International*, 160(1), (2005), 388-412.

Faulkner, D. R., Jackson, C. A. L., Lunn, R. J. et al.: A review of recent developments concerning the structure, mechanics and fluid flow properties of fault zones, *Journal of Structural Geology*, 32(11), (2010), 1557-1575.

Garibaldi, C., Guillou-Frottier, L., Lardeaux, J. M., Bonté, D., Lopez, S., Bouchot, V., Ledru, P.: Thermal anomalies and geological structures in the Provence basin: Implications for hydrothermal circulations at depth, *Bulletin de la Société Géologique de France*, 181(4), (2010), 363-376.

Guillou-Frottier, L., Duwiquet, H., Launay, G., Taillefer, A., Roche, V., Link, G.: On the morphology and amplitude of 2D and 3D thermal anomalies induced by buoyancy-driven flow within and around fault zones, *Solid Earth*, 11(4), (2020),1571-1595.

Guillou-Frottier, L., Carré, C., Bourgine, C., Bouchot, V., Genter, A.: Structure of hydrothermal convection in the Upper Rhine Graben as inferred from corrected temperature data and basin-scale numerical models, *Journal of Volcanology and Geothermal Research*, 256, (2013), 29-49.

Heap, M. J. and Kennedy B. M.: Exploring the scale-dependent permeability of fractured andesite, *Earth and Planetary Science Letters*, 447, (2016), 139-150.

Horne, R. N.: Three-dimensional natural convection in a confined porous medium heated from below, *Journal of Fluid Mechanics*, 92(4), (1979), 751-766.

Ingebritsen, S. E., & Gleeson, T.: Introduction to the special issue on crustal permeability. *Geofluids*, 15, (2015), 1-10.

Lorenzini, G., Moretti, S., & Conti, A.: Fin shape thermal optimization using Bejan's constructal theory, *Synthesis Lectures on Engineering*, 6(1), (2011), 1-219.

Lucazeau, F., and Vasseur, G.: Heat flow density data from France and surrounding margins, *Tectonophysics*, 164(2-4), (1989), 251-258.

Lucazeau, F.: Flux de chaleur, production de chaleur et évolution géodynamique récente du Massif Central Français. 1981. Thèse de doctorat.

Ma, Y., Wang, G., Yan, R., Wang, B.: Long-term In Situ Permeability Variations of an Active Fault Zone in the Interseismic Period. *Pure and Applied Geophysics*, 176(12), (2019), 5279-5289.

Martel, S. J.: Formation of compound strike-slip fault zones, Mount Abbot quadrangle, California, *Journal of Structural Geology*, 12(7), (1990), 869-882.

Magri, F., Möller, S., Inbar, N., Möller, P., Raggad, M., Rödiger, T., ... & Siebert, C.: 2D and 3D coexisting modes of thermal convection in fractured hydrothermal systems-Implications for transboundary flow in the Lower Yarmouk Gorge, *Marine and Petroleum Geology*, 78, (2016), 750-758.

Magri, F., Cacace, M., Fischer, T., Kolditz, O., Wang, W., Watanabe, N.: Thermal convection of viscous fluids in a faulted system: 3D benchmark for numerical codes. Energy Procedia, 125, (2017), 310-317.

Mazabraud, Y., Béthoux, N., Guilbert, J., Bellier, O.: Evidence for short-scale stress field variations within intraplate central-western France, *Geophysical Journal International*, 160(1), (2005), 161-178.

Mitchell, T. M., and Faulkner, D. R.: Towards quantifying the matrix permeability of fault damage zones in low porosity rock,. *Earth and Planetary Science Letters*, 339, (2012). 24-31.

Parisio, F., Vilarrasa, V., Wang, W., Kolditz, O., Nagel, T.: The risks of long-term re-injection in supercritical geothermal systems. *Nature Communications*, 10(1), (2019), 1-11.

Parry, W. T., Wilson, P. N., Bruhn, R. L.: Pore-fluid chemistry and chemical reactions on the Wasatch normal fault, Utah, *Geochimica et Cosmochimica Acta*, 52(8), (1988), 2053-2063.

Reis, A. H.: Constructal theory: from engineering to physics, and how flow systems develop shape and structure. (2006), 269-282.

Roche, V., Sternai, P., Guillou-Frottier, L., Menant, A., Jolivet, L., Bouchot, V., & Gerya, T.: Emplacement of metamorphic core complexes and associated geothermal systems controlled by slab dynamics, *Earth and Planetary Science Letters*, 498, (2018) 322-333.

Scibek, J.: Multidisciplinary database of permeability of fault zones and surrounding protolith rocks at world-wide sites, *Scientific Data*, 7(1), (2020), 1-14.

Sibson, R. H., Robert, F., & Poulsen, K. H.: High-angle reverse faults, fluid-pressure cycling, and mesothermal gold-quartz deposits. *Geology*, 16(6), (1988), 551-555.